Earth and Planetary Science Letters 618 (2023) 118274

Contents lists available at ScienceDirect

Earth and Planetary Science Letters

journal homepage: www.elsevier.com/locate/epsl

Islands of chaos in a sea of periodic earthquakes

Judith Gauriau *, Sylvain Barbot, James F. Dolan

Department of Earth Sciences, University of Southern California, 3651 Trousdale Parkway, Los Angeles, CA 90089, USA

ARTICLE INFO

Article history:
Received 12 January 2023
Received in revised form 1 June 2023
Accepted 9 June 2023
Available online 11 July 2023
Editor: R. Bendick

Keywords:
quasi-periodic
paleoseismic record
frictional parameters
recurrence time interval
coefficient of variation
chaotic

ABSTRACT

Long paleoseismic records on mature faults suggest potentially chaotic recurrence patterns with cycles of strain accumulation and release that challenge simple slip- or time-predictable recurrence models. In apparent contradiction, the relatively small variability of earthquake recurrence times on these faults is often characterized as *quasi-periodic*, implying much regularity in the underlying mechanics. To reconcile these observations, we simulate one of the longest paleoearthquake records – the 24-event record from the Hokuri Creek site on the Alpine fault in New Zealand – using a physical model of rate- and state-dependent friction. In a parameter space formed by three non-dimensional parameters, a sea of parameters produces periodic earthquake recurrence behavior. Only a few models are characterized by fundamentally aperiodic recurrence patterns, in parametric islands of chaos. Complex models that produce partial and full ruptures of the Alpine fault can explain the earthquake recurrence behavior of the Alpine fault, reproducing up to 11 consecutive events of the Hokuri Creek paleoseismic record within uncertainties. The breakdown of the slip- and time-predictable recurrence patterns occurs for faults that are much longer than the characteristic nucleation size. The quasi-periodicity of seismic cycles is compatible with the nonlinear and potentially chaotic underlying mechanical system, posing an inherent challenge to long-term earthquake prediction.

1. Introduction

Our understanding of the recurrence pattern of large earthquakes relies on paleoseismic records, which, in exceptional cases, span prolonged periods, as for the Dead Sea fault, with 12 recognized events in the past 14,000 years (Ferry et al., 2011), the San Andreas fault (SAF) at Wrightwood, with 15 characterized events since ca. 500 CE (Weldon et al., 2004), and the San Jacinto fault at Hog Lake, with 21 events documented since 1,800 BCE (Rockwell et al., 2015). In those studies, the seismic cycle is often characterized by the coefficient of variation (CoV) of the recurrence times, associated with quasi-periodic (CoV$<$1), random (CoV $\sim$ 1) or clustered (CoV $>$ 1) events (e.g., Kagan and Jackson, 1991). For example, the Dead Sea fault is characterized by earthquake recurrence times ranging from random to clustered (Marco et al., 1996), whereas other faults reveal quasi-periodic behavior, such as the San Jacinto fault's record at Hog Lake with a CoV of the recurrence times of 0.57 (Rockwell et al., 2015). Similarly, the San Andreas fault's recurrence behavior at Wrightwood is quasi-periodic, with a CoV $\sim$ 0.7 (Scharer et al., 2011), and the SAF Carrizo Plain section is characterized by a CoV of earthquake recurrence of $\sim$0.5 (Akçiz et al., 2010).

The evolution of the slip deficit, i.e., the difference between the expected slip based on the average loading rate and the actual slip per event, provides another means of characterizing the recurrence pattern (Shimazaki and Nakata, 1980). For a slip-predictable behavior, the final stress is constant, but the initial stress can vary from event to event, implying a correlation between recurrence time and displacement between two successive earthquakes. Time-predictable behavior occurs when the amount of time following an earthquake depends upon its size, implying rupture initiation at a fixed yield stress. Testing the validity of the time- or slip-predictable models in nature requires pairing records of paleo-earthquake ages with slip-per-event data. Slip-predictable behavior has been shown in a few locations with relatively short records. For instance, both the Carrizo Plain record, based on the six most-recent earthquakes (Akçiz et al., 2010), and the slip history of the North Anatolian fault, based on the displacements and ages of the past four major earthquakes (Kondo et al., 2010), suggest slip-predictable earthquake behavior. However, the time-predictable model has been systematically rebutted in other cases (e.g., Wechsler et al., 2014).

The quasi-periodic behavior of earthquakes is often interpreted to indicate regularity in the underlying fault mechanics, imply-

* Corresponding author.
E-mail address: gauriau@usc.edu (J. Gauriau).

https://doi.org/10.1016/j.epsl.2023.118274
0012-821X/

ing bounds on the dynamics or persistent mechanical conditions within the fault zone. Conversely, if paleoseismic records deviate from the time-predictable and slip-predictable models, this suggests non-stationary physical conditions, such as changing loading rate or fault microstructure, affecting rupture nucleation and propagation from one event to the next. This conundrum is perhaps best exemplified by the 24-event, 7,900-year-long, Hokuri Creek (HC) paleoseismic record on the Alpine fault in New Zealand, one of the longest ever produced. The catalog features seismic events every 329 ± 68 years ($\pm 1\sigma$; Fig. 1c) with a very low CoV of $\sim$0.3 (Berryman et al., 2012), qualifying the southwestern Alpine fault as quasi-periodic (Fig. 1b, c). Despite the relatively regular recurrence pattern, inferred slip-per-event data suggest that the HC paleoseismic record departs markedly from both behaviors predicted by time- and slip-predictable models (Fig. 1d). The record is actually characterized by internal variability of pre- to post-event recurrence time (Fig. 1e).

These observations raise fundamental questions: What are the underlying mechanics responsible for an apparently periodic seismic cycle that 1) breaks the slip- and time-predictable patterns, 2) produces a relatively broad range of recurrence intervals, and 3) can be characterized by a low CoV? To address these questions, we use numerical simulations to explore the physical parameters that control the recurrence pattern of earthquakes on the Alpine fault. We identify the physical conditions most compatible with the paleoseismic record at the HC site. When the fault is sufficiently unstable, the recurrence patterns evolve from periodic to aperiodic. The transition involves repeating cycles of multiple earthquakes, whereas the truly aperiodic sequences result from deterministic chaos. Some of these models can explain the most consecutive events – more than even documented in most other paleoseismic records – while featuring a low CoV and digressing from the slip- and time-predictable models. Finally, we discuss the possible underlying causes for the earthquake recurrence behavior of the Alpine fault.

2. Methods

We build numerical simulations to reproduce the sizes and recurrence patterns of paleo-earthquakes documented at the Hokuri Creek site. We use a 2D approximation in condition of in-plane strain relevant to long, isolated strike-slip faults, such as the Alpine fault. We assume a physical model of rate- and state-dependent friction in isothermal conditions and use the constitutive relationships governing slip along the fault over multiple seismic cycles (Barbot, 2019a,b). The governing equations and constitutive parameters used to model the Alpine fault are detailed in the Supplemental Material (SM). We model the 400-km-long, structurally isolated, southwestern Alpine fault as a velocity-weakening fault with a proxy for the HC site located at 100 km from the southwestern end of the fault (Fig. 2). The fault is loaded at a uniform rate of 23 mm/yr, in agreement with both the long-term slip-rate of the southwestern section of the Alpine fault (Berryman et al., 1992; Sutherland et al., 2006), and the average recurrence intervals of the HC paleoseismic record, i.e., 329 ± 129 years ($\pm 2\sigma$) (Berryman et al., 2012), combined with the assumed amount of slip per event (see discussion in SM and references therein).

In a preliminary exploration of model parameters (Fig. S1), we find that the effective normal stress $\overline{\sigma} = 13$ MPa captures the average recurrence time of earthquakes at HC (Fig. S2). We explore the role of the remaining physical properties of the fault zone to explain the temporal variability of the paleoseismic record. To generalize our findings to various combinations of physical properties of the fault zone, we explore three non-dimensional parameters that are key to the resolution of the seismic cycle, controlling the rupture style and recurrence patterns (Barbot, 2019b; Nie and Barbot, 2022): the Dieterich-Ruina-Rice number R_u, the R_b number, and the static coefficient of friction μ_0 (details in Fig. 2 and SM). The Dieterich-Ruina-Rice number can be interpreted as the ratio of the fault length, W, to a characteristic nucleation size, h^*, that controls the dynamics of the ruptures:

$$R_u = \frac{(b-a)\,\overline{\sigma} W}{GL} \approx \frac{W}{h^*},$$

where G is the rigidity of the surrounding rocks and L is the characteristic weakening distance of rate- and state-dependent friction (Dieterich, 1979; Rice and Ruina, 1983; Ruina, 1983). The sign of $(b-a)$ characterizes whether the friction is velocity-strengthening or velocity-weakening at steady state. Smaller-scale instabilities typically develop for increasing R_u values (Cattania, 2019; Barbot, 2019b). The R_b number is the ratio of dynamic and static stress drops:

$$R_b = \frac{b-a}{b}.$$

This ratio controls the importance of the transient weakening and strengthening effects, as well as the nucleation style and the emergence of slow-slip events (Rubin and Ampuero, 2005; Nie and Barbot, 2021). The reference static coefficient of friction μ_0 is the ratio of the shear stress to the normal stress measured at steady-state at a reference velocity. The reference friction coefficient affects the dynamics of rupture and is poorly known in nature, and usually fixed in earthquake simulation studies (e.g., Barbot, 2019b; Sathiakumar and Barbot, 2021; Nie and Barbot, 2022). In this study, we explore possible values of μ_0 within a range applicable to seismic events.

We perform numerical simulations using the spectral boundary-integral method with adaptive time steps and the radiation-damping approximation to resolve all phases of the seismic cycle (Barbot, 2021).

To keep the model exploration tractable, we use the following strategy: We first explore the set of parameters R_u and μ_0 for a fixed $R_b = 0.286$, a value typical of fault zones derived from laboratory experiments (Tse and Rice, 1986; Blanpied et al., 1995). We then jointly explore the R_b and R_u numbers using a friction coefficient μ_0 selected from the previous step. For each combination of parameters, we conduct 20,000-year-long simulations and analyze the behavior of the fault after a few thousand years to mitigate the effects of the initial conditions (e.g., Barbot, 2020; Sathiakumar and Barbot, 2021). For each simulation, we select the 24-earthquake interval in the remaining period that best explains the HC record.

3. Results

We first examine the earthquake recurrence patterns that emerge in the parameter space (Fig. 3). We document the periodicity of earthquake cycles based on recurrence times alone, irrespective of the amount of slip, rupture velocity, or other source mechanisms. We consider slip events as earthquakes if the peak velocity exceeds 1 mm/s. Under most conditions, the seismic cycle converges to a repeat cycle consisting of one or more earthquakes, which we refer to as period-n cycles, where n is the smallest number of earthquakes that form a repeat sequence. The different types of earthquake recurrence time behavior are exemplified in Figs. 3c to 3h and in Fig. S3.

In the $\{R_u; \mu_0\}$ parameter space, truly periodic behavior (period-1) that follows the time- and slip-predictable models is observed for low R_u values (10 to 30), at different μ_0 values, as well as for R_u values spanning 50 to 95 for relatively low friction

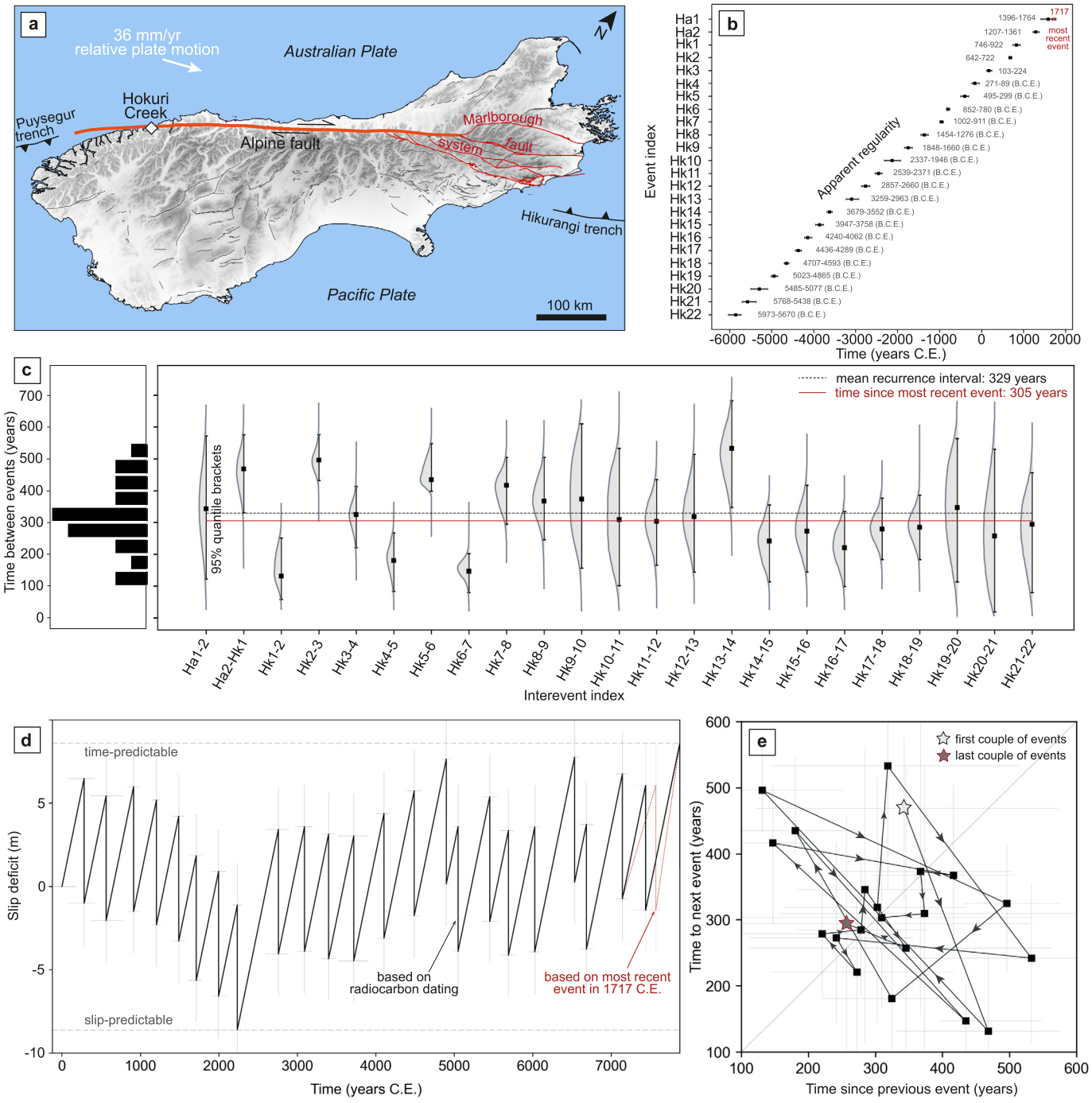

Fig. 1. Overview of the Hokuri Creek (HC) paleoseismic site and data (modified after Berryman et al. (2012)). (**a**) Location of the HC paleoseismic site within the Alpine fault system, New Zealand (Langridge et al., 2016). (**b**) Ages of 24 surface-rupturing earthquakes on the Alpine Fault at HC. Intervals are the 95% brackets inferred from radiocarbon ages. The red cross refers to the most recent event (MRE) in 1717 C.E. (De Pascale and Langridge, 2012). (**c**) Recurrence time intervals, with probability density functions. (**d**) Slip deficit of the HC record through time, with inferred average slip per event of 7.5 ± 2.5 m, and its relation to the time-predictable (upper bound) and slip-predictable (lower bound) models, as defined by Shimazaki and Nakata (1980). (**e**) Plot of the time to succeeding event against the time since preceding event for the HC record.

coefficients (Fig. 3a). Truly aperiodic behavior, i.e., deterministic chaos, appears in isolated islands of parameters and in a somewhat larger model space for R_u between 45 and 55 and μ_0 between 0.40 and 0.55. Other cases that deviate from the time- and slip-predictable models represent period-n behavior, i.e., period-n cycles with $n > 1$. Similarly, truly periodic behavior is observed within large sections of the $\{R_u; R_b\}$ parameter space, and chaotic behaviors appear in isolated patches (Fig. 3b).

We aim to quantitatively explain the recurrence times at HC within the explored parameter space, which will naturally produce low CoV and a set of events that resembles the succession of paleoearthquakes of the HC record. We therefore compare the numerical simulations of seismic cycles with the HC paleoseismic record. To mitigate any bias in recurrence times from aftershocks and other small earthquakes, we trim the simulated sequences according to paleoseismic assumptions. Those assumptions tackle: 1) the timing of successive earthquakes, i.e., two earthquakes occurring within a brief amount of time will not necessarily be distinguishable in the stratigraphy, and 2) the amount of slip per event, i.e., a small-magnitude event might not be recorded in the stratigraphy

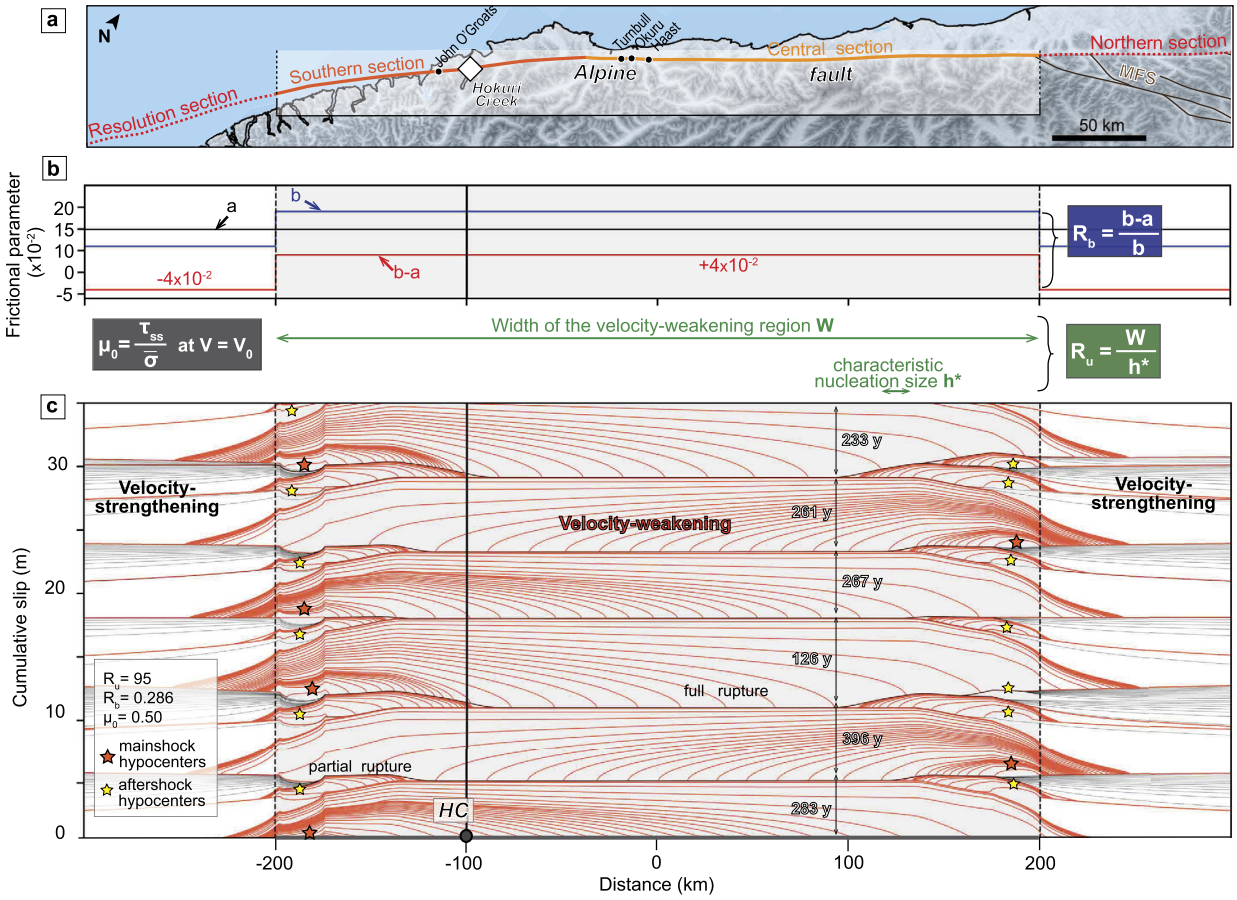

Fig. 2. Representation of the Alpine fault zone model with a reference map (**a**) indicating the location of the Hokuri Creek site. (**b**) Distribution of the rate dependence at steady state b-a and parameters a and b throughout the total modeled length of the fault. (**c**) Example plot of the cumulative slip along the fault for $R_u = 95$, $R_b = 0.286$, and $\mu_0 = 0.50$. The cumulative slip is plotted for a total of 17 events in the selected simulation, between years 12,285 and 13,714 (within a whole 20,000-year-long simulation). A proxy for the location of HC is shown and the vertical line above it shows where the sampling is done. The orange isochrons feature cumulative coseismic slip every 20 seconds, and the gray contours show slip isochrons every 20 years in the interseismic periods.

(see further details in SM). We then compare the newly obtained catalog of recurrence times with the HC data. For each simulation, we select the sequence of 23 recurrence times that features the maximum number of successive recurrence times falling within the 95% confidence intervals of the HC record. This conservative criterion is used to discard models that explain data for short, isolated intervals and to account for uncertainties in the paleoseismic record. The results are displayed in Fig. 4 for the parameter spaces R_u and μ_0 at fixed $R_b = 0.286$ (Fig. 4a) and for R_u and R_b at fixed $\mu_0 = 0.50$ (Fig. 4b), correspondingly to Fig. 3.

The best fit models occur for period-2 behaviors (Fig. 3a), at $\{R_u = 75;\ \mu_0 = 0.60\}$ and $\{R_u = 80;\ \mu_0 = 0.50$ and $0.55\}$ for fixed $R_b = 0.286$, as well as for $\{R_u = 50;\ R_b = 0.50\}$ for fixed $\mu_0 = 0.50$ (Fig. 3b), with 13 successive recurrence times that fall within the 95% confidence intervals of the HC record. Two of these best-fitting models are displayed in Figs. 4c to 4f. Other good fit models produce 11 or 10 successive recurrence times within the 95% confidence intervals of the observations. This occurs for $\{R_u = 90;\ R_b = 0.50;\ \mu_0 = 0.50\}$, corresponding to a period-2 behavior, and for $\{R_u = 100;\ R_b = 60;\ \mu_0 = 0.50\}$ corresponding to a chaotic behavior (Fig. 4b), as well as for the simulations with parameters $\{R_u = 60;\ \mu_0 = 0.60;\ R_b = 0.286\}$, exhibiting a period-11 behavior, $\{R_u = 90;\ \mu_0 = 0.60;\ R_b = 0.286\}$, characterized by a period-5 behavior and $\{R_u = 95;\ \mu_0 = 0.50;\ R_b = 0.286\}$, showing deterministic chaos.

Since the behavior of the Alpine fault at HC is neither slip-predictable, nor time-predictable (Fig. 1e), and since the earthquake recurrence time is not perfectly constant (CoV of 0.3), we should rule out any type of model that manifests true periodicity (equivalent to CoV = 0) (Fig. 1e). Therefore, we further select the models with a distribution of recurrence times most compatible with the HC record in a statistical sense. We perform two-sample Kolmogorov-Smirnov tests between the HC data and the selected best sequences of 23 recurrence times, i.e., the ones that feature the maximum number of successive recurrence times falling within the 95% uncertainties of the HC record, in order to test if the two populations come from the same distribution. Our working null hypothesis H_0 is that the two populations were drawn from the same distribution. We look at the related p-values (i.e., the probability that the Kolmogorov-Smirnov statistic is larger than the maximum difference between the cumulative distributions of the two samples, assuming H_0 is true) for each of the performed tests and display them in the explored parameter spaces in Figs. 5a and 5b (correspondingly to Figs. 3a, 3b, 4a, and 4b). The smaller the p-value, the smaller the probability of making an error by rejecting H_0. In other words, higher p-values relate to recurrence time interval distributions that are closer to the distribution of HC recurrence times.

The overlap of the best models shown in Figs. 4a and 4b with the highest p-values shown in Figs. 5a and 5b helps us narrow down the allowable frictional parameter space that best explain the HC record. With this additional consideration, we find that the best simulations are obtained for $\{R_u = 90;\ \mu_0 = 0.60;\ R_b = 0.286\}$, characterized by a period-5 behavior, and $\{R_u = 95;$

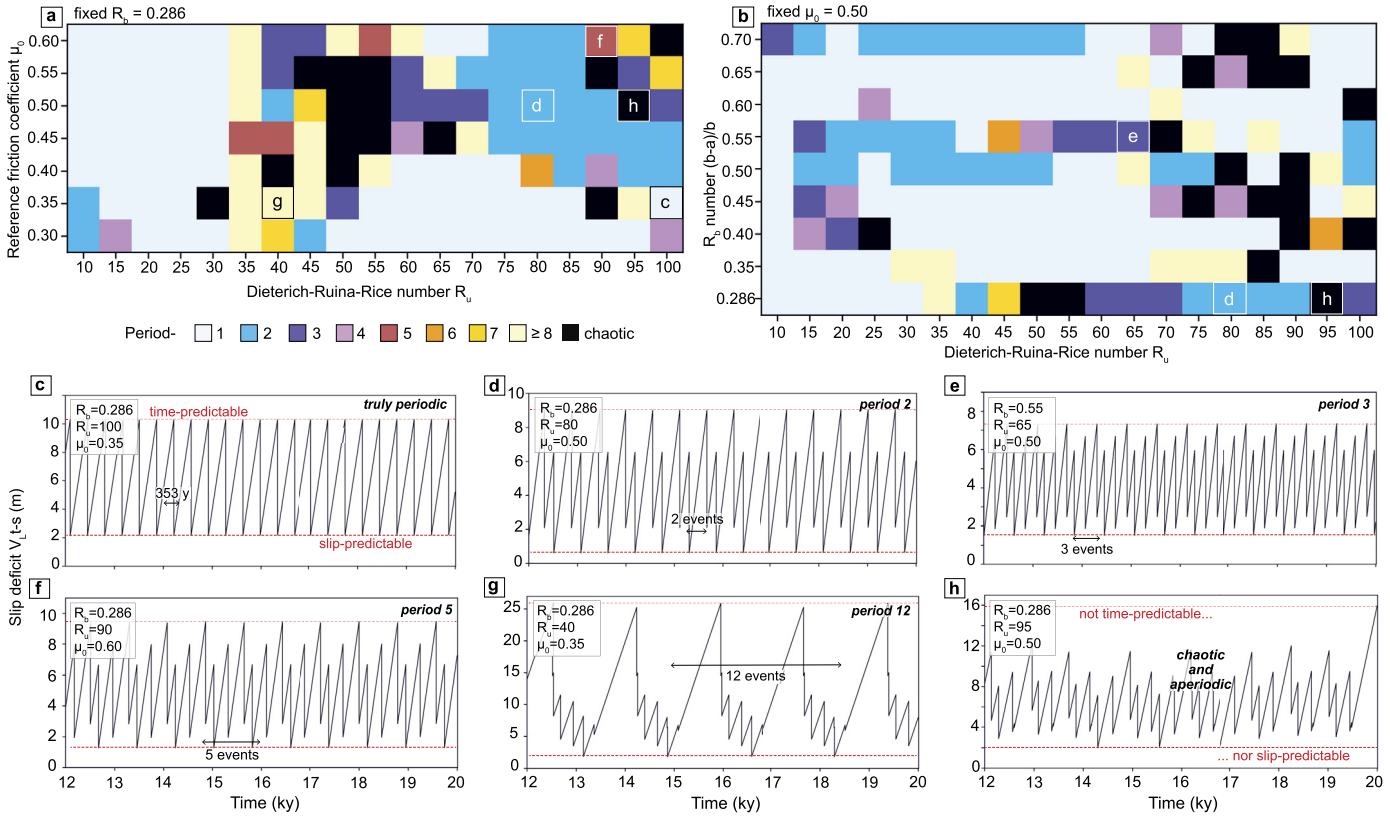

Fig. 3. Overview of the periodicity styles obtained for =13 MPa in the parameter spaces formed by R_u and μ_0 and by R_u and R_b at the sampling point (marked HC in Fig. 2c). In (**a**) and (**b**), each color refers to a type of earthquake repeat time periodicity, and insets (**c**) to (**h**) show the evolution of slip deficit through time for the last 8,000 years of the whole simulation. (**f**) refers to the period-5 model that fits well the HC data, using both ranking criteria we use in Figs. 5c and 5d. (**h**) refers to the chaotic model, also shown in Figs. 2c, 5e, and 5f, that fits the HC data well, using both ranking criteria.

$\mu_0 = 0.50$; $R_b = 0.286\}$, showing chaotic behavior. The period-5 model explains 10 successive recurrence times (i.e., 11 successive events from interval Hk8-9 to interval Hk17-18), and a total of 16 disconnected recurrence intervals that fall within the 95% uncertainties of the HC record. The mean recurrence time of the 24-event selected sequence for this model is 307 ± 102 years, corresponding to a CoV of 0.33, which falls within the 1σ confidence interval of the mean recurrence time found at HC (Berryman et al., 2012). Similarly, the chaotic model explains 10 successive recurrence times (i.e., 11 successive events from interval Hk12-13 to interval Hk21-22), a total of 15 disconnected recurrence intervals that fall within the 95% uncertainties of the HC record, and the scattered nature of pre- and post-event intervals (Fig. 4c, d). The mean recurrence time of the simulated 24-event record for this chaotic model is 277 ± 105 years, corresponding to a CoV of 0.38, which falls within the 1σ confidence interval of the mean recurrence time found at HC, characterized by a CoV of ~0.3 (Berryman et al., 2012).

4. Discussion

Our study suggests that seismic cycles with low CoV that break the time- and slip-predictable end-member recurrence models are related to the nonlinear dynamics of the fault system. The two best-fitting models that explain the most consecutive events and produce a distribution of recurrence times that most resemble the HC record produce period-5 sequences or aperiodic deterministic chaos. Multiple-periodic cycles are generally understood as transitional behavior toward chaotic cycles. For example, the transition from periodic events to deterministic chaos in a Lorenz attractor involves bifurcations with period-doubling (Lorenz, 1963). Nonlinear dynamic systems showing a period-3 recurrence pattern (see an example in Fig. 3e) are capable of chaotic behavior (Li and Yorke, 2004). Our results support previous studies that interpret earthquake recurrence as chaotic in historical catalogs (Huang and Turcotte, 1990; Ito, 1980; Iliopoulos and Pavlos, 2010), earthquake sequences (Shelly, 2010; De Santis et al., 2010), and laboratory earthquakes (Gualandi et al., 2023). Chaotic sequence of earthquakes can be due to the complexity of the rate- and state-dependent friction law in spring-slider systems (Becker, 2000; Erickson et al., 2008) and appear in continuum models for sufficiently small nucleation (Kato, 2014; Cattania, 2019; Barbot, 2019b; Nie and Barbot, 2022).

The two best models in the parameter space explored in this study are found for $\{R_u = 90;\ \mu_0 = 0.60;\ R_b = 0.286\}$, characterized by a period-5 behavior, and $\{R_u = 95;\ \mu_0 = 0.50;\ R_b = 0.286\}$, showing chaotic behavior. These parameters suggest that the Alpine fault is characterized by a small nucleation size relative to its overall length and by a friction coefficient compatible with Byerlee's law (Byerlee, 1978). Although the structural maturity of the Alpine fault would suggest a lower friction coefficient in the seismogenic zone (Collettini et al., 2009; Boulton et al., 2017; Copley, 2018), rocks cored from the central section in the Deep Fault Drilling Project reveal friction coefficients of 0.50–0.75 at the relevant temperatures (Boulton et al., 2012, 2014; Ikari et al., 2014; Valdez et al., 2019), compatible with our findings.

The R_u and R_b numbers control the relative amplitude of different energy sources and sinks during seismic rupture, i.e., fracture energy, heat, and radiated energy (Kanamori and Rivera, 2006), by affecting the amount of weakening and the slip-weakening distance, which directly alters the fracture energy. The trade-off between R_b and R_u displayed in Figs. 4b, S5, S9, and S10 indicates an upper bound on the fracture energy: For sufficiently large frac-

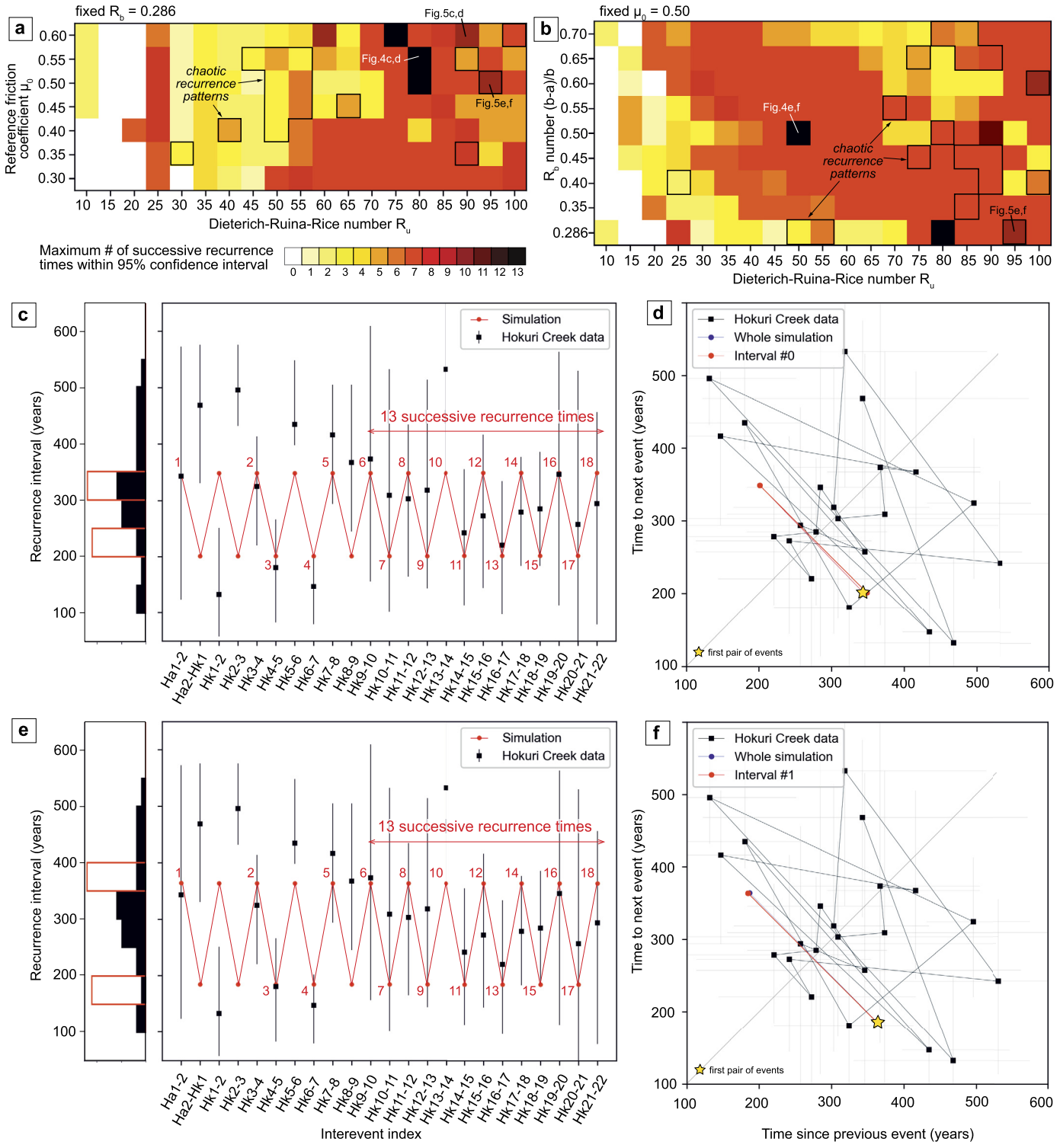

Fig. 4. Results of fitting of best sequences of 23 recurrence intervals to the Hokuri Creek paleoseismic data (**a**) for the parameter spaces formed by R_u and μ_0 and (**b**) by R_u and R_b. (**a**) and (**b**) display the highest number of successive recurrence intervals that fall within the 95% confidence intervals of the HC paleoseismic time recurrence intervals for each simulation. The best results are obtained for simulations with a period-2 earthquake recurrence behavior (shown as black squares), and are displayed in insets (**c**) to (**f**). (**c**) shows the recurrence time sequence of the selected interval for the period-2 simulation of parameters $R_u = 80$, $\mu_0 = 0.55$, $R_b = 0.286$, compared with the HC data. For this selected sequence, the CoV is 0.264 and the average recurrence time is 277.9 yr. (**d**) shows the entire 20,000-year-long simulation for the preferred chaotic model and the selected interval in light of the HC data. (**e**) and (**f**) show the same series of plots for period-2 simulation of parameters $R_u = 50$, $\mu_0 = 0.50$, $R_b = 0.50$. This selected sequence is characterized by a CoV of 0.322 and an average recurrence time interval of 278.0 yr.

ture energy per unit area during rupture, the complex recurrence patterns of HC cannot be reproduced, whether it is due to a large weakening distance (small R_u) or a large direct effect (small R_b). This suggests that the Alpine fault earthquakes dissipate relatively little energy in fracture, diverting it instead into seismic radiation and heat.

The small nucleation patch size for the Alpine fault implies a wide range of possible earthquake sizes. For instance, when $R_u =$

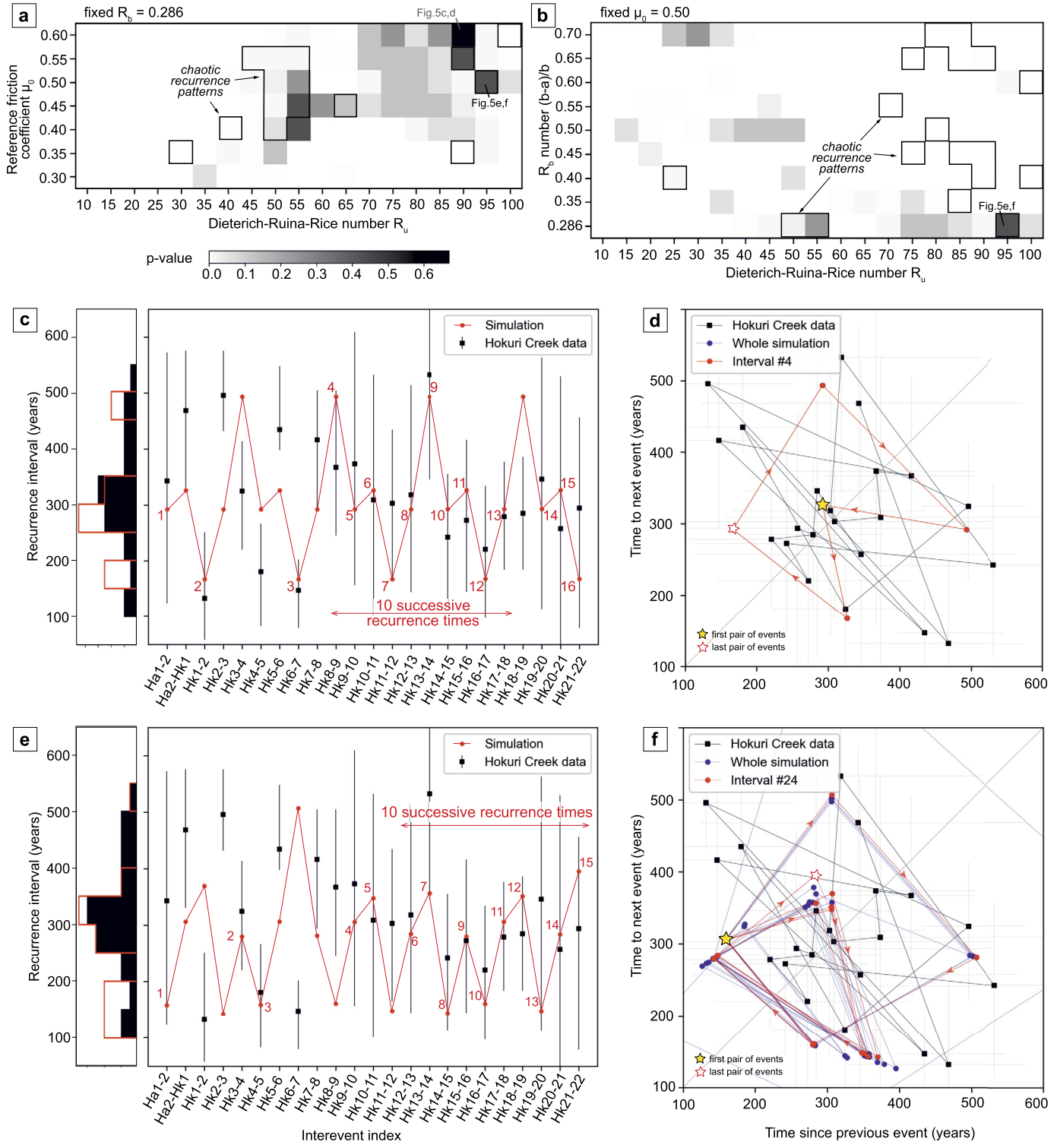

Fig. 5. Additional method for ranking the selected sequence of 23 intervals (Fig. 4), with the use of p-values of the related tested null-hypothesis H_0: "The HC record and the selected simulated record were drawn from the same distribution", using a two-sample Kolmogorov-Smirnov test. The p-values are displayed in (**a**) for the parameter space formed by R_u and μ_0 and in (**b**) for the parameter space formed by R_u and R_b. The highest p-value is obtained for the simulation of parameters $R_u = 90$, $R_b = 0.286$, and $\mu_0 = 0.60$, characterized by a period-5 recurrence time behavior, which also has a good fit with the HC data, using the ranking criterion of Fig. 4. Insets (**c**) and (**d**) show the recurrence time sequence of the selected interval for this period-5 model, compared to the HC record. For this sequence, the CoV is 0.333 and the average recurrence time is 307.4 yr. The other simulation that gathers a high p-value and a large number of successive recurrence times falling within 95% uncertainties of the HC record is the chaotic simulation of parameters: $R_u = 95$, $R_b = 0.286$, and $\mu_0 = 0.50$. (**e**) and (**f**) show the recurrence time sequence of the selected interval for this chaotic model, compared to the HC record. For this selected sequence, CoV = 0.380, the average repeat recurrence time is 277.4 yr.

95, the smallest allowable rupture size (~7 km) represents 2% of the fault length. Although most simulated earthquakes for both models represent unilateral ruptures of the entire fault (Figs. 2c and S1b), a few ruptures break segments of less than 100 km length, only a few of which reach the HC site. Consistent with this observation, the paleoseismic record of large-magnitude earth-

quakes shows that the Alpine fault does not generate frequent earthquakes that are less than a $M_w \sim 7$ range, except for aftershocks. Indeed, the magnitudes of the paleo-seismic events are assumed to be on the same order of the most recent event ($M_w = 8.1$–8.3) and antepenultimate ($M_w = 7.6$) Alpine fault earthquakes (Sutherland et al., 2007; De Pascale and Langridge, 2012). Full-length ruptures of the entire Alpine fault are probably the dominant means by which the seismic moment of the fault is released. The last three events that occurred at HC correlate with the well-constrained ages of ruptures along the central section of the Alpine fault (Howarth et al., 2016), suggesting that the most-recent event (MRE) in 1717 C.E., as well as the penultimate and antepenultimate events ruptured both the Central and Southern sections. The MRE not only ruptured those sections, but also potentially the southern end of the Alpine fault's northern section, with a calculated magnitude M_w 8.1–8.3 and a rupture length of ∼410–450 km (Yetton and Nobes, 1998; Stirling et al., 2012; De Pascale and Langridge, 2012; Cochran et al., 2017; Howarth et al., 2018). However, the time ranges of older events recorded at the HC and John O'-Groats sites on the Southern section do not match those recorded at Lake Ellery on the Central section (Fig. 2a), indicating that the ruptures recorded on the Southern section did not simultaneously rupture the Central section as well, and vice versa. This suggests that ruptures do not consistently break the entire length of the fault. Specifically, 52% of the events recognized on the Alpine fault are restricted to either the Southern section or the Central section, whereas 48% of the events rupture both sections at the same time (Howarth et al., 2016, 2018; Cochran et al., 2017).

The average earthquake recurrence intervals found for the two best fit models (277 ± 105 years for the chaotic model and 307 ± 102 years for the period-5 model) are somewhat shorter than the average recurrence interval documented by Berryman et al. (2012) at HC (329 ± 68 years), although they are not significantly different at the 1σ confidence interval. Some paleoseismic studies at other sites on the southwestern Alpine fault have revealed shorter average recurrence intervals, such as (1) 291 ± 23 years (CoV = 0.41) for the combination of HC ages and the seven paleoearthquake ages obtained at John O'Groats wetland (Fig. 2a), 25 km south of HC (Cochran et al., 2017); and (2) 263 ± 63 years (CoV = 0.26) on the Central section of the Alpine fault, starting less than 100 km north of the HC site, based on the evidence of the eight most-recent earthquakes (Howarth et al., 2018). For similar amounts of slip per event to that inferred in our work at the HC site (7.5 m/event), the recurrence time intervals resulting from these other sites would require a faster slip rate than the average loading rate used in our study (23 mm/yr). For instance, Cochran et al. (2017) used the ∼28 mm/yr long-term slip rate from Barth et al. (2014), which was based on restoration of ∼270 ka glacial deposits displaced by the Alpine fault.

This bias could be recovered by employing a different long-term slip rate, which would have minimal consequences for the seismic cycle behavior beyond changing the recurrence time of earthquakes, but would be incompatible with the well-constrained incremental slip-rate record of Sutherland et al. (2006) which was measured over four separate displacement intervals and pertains directly to the section of the fault containing the HC site. Perhaps other additional physical processes could help to reconcile our results with both the actual distribution of recurrence intervals obtained at HC, and the recurrence intervals observed at other sites along the Alpine fault. The frictional evolution of the fault may involve enhanced weakening mechanisms, such as flash weakening (Beeler et al., 2008), thermal decomposition (Sulem and Famin, 2009), thermal pressurization (Noda and Lapusta, 2013), or additional thermal effects that modulate strength throughout the seismic cycle (Wang and Barbot, 2020, 2023; Barbot, 2022). Internal structural complexity of the Alpine fault may also affect the recurrence patterns (Howarth et al., 2021). Another reason why it is difficult to obtain a simulated sequence that gives an average time recurrence interval close to the one of HC is that the variability of the record comes mainly from the eight most-recent events, for which the recurrence intervals vary more (CoV = 0.37) than for the whole record. In contrast, the 15 oldest recurrence intervals in the HC record indicate more regular earthquake occurrence, with a very low CoV of 0.24.

The numerical simulations obtained from this study provide further insights into the possible underlying mechanics of seismic cycles that deviate from the time- and slip-predictable models. For a high R_u number, the nucleation size is small enough to generate full and partial ruptures of the seismogenic zone due to heterogeneous stress accumulation along the fault. The partial ruptures delay the nucleation of the subsequent through-going ruptures, breaking the simple time-predictable pattern. To first order, the fault slip produced during a seismic event is controlled by the rupture length. Consequently, partial ruptures also create variability in the slip of individual earthquakes, even at uniform stress drops, breaking the slip-predictable pattern, as well. Finally, partial ruptures leave behind stress concentrations that will affect subsequent ruptures. As the stress inherited from previous ruptures affects the initial condition of any subsequent rupture, a sequence of earthquakes yields an increasingly complex stress distribution along the fault. As a result, a period-5 model, like the one obtained with parameters $\{R_u = 90;\ \mu_0 = 0.60;\ R_b = 0.286\}$ accomplishes these complex conditions, and represents an intermediate step towards a fully aperiodic, chaotic system, as represented by the second model obtained with parameters $\{R_u = 95;\ \mu_0 = 0.50;\ R_b = 0.286\}$. Under some conditions, as the ones reached in that latter model, the cycle becomes aperiodic. As the average recurrence time remains controlled by the structural properties of the fault zone that evolve at time scales much longer than the seismic cycle – fault length, structural maturity, and the distant boundary conditions of tectonic plates (e.g., Gauriau and Dolan, 2021) – a chaotic seismic cycle such as the one we found still operates within reasonable bounds, leading to a low CoV.

5. Conclusions

We explore a wide range of frictional parameters to model the *quasi-periodic* earthquake recurrence pattern of the Alpine fault's Hokuri Creek paleoseismic record. A sea of parameters produces strictly periodic or period-n cycles of earthquakes. Only a few islands of parameters within the entire explored space yield chaotic seismic cycles that break the time- and slip-predictable recurrence patterns and produce low variations of recurrence times. Two models that explain the Hokuri Creek paleoseismic record exhibit period-5 and chaotic behaviors, respectively, both of which are the trademark of nonlinear fault dynamics. These models feature a highly unstable fault with a length much greater than a characteristic nucleation size, and Byerlee-like friction coefficients. The compatibility of the quasi-periodicity of seismic cycles with a complex underlying mechanical system poses an intrinsic obstacle to long-term earthquake prediction, even if the fundamental laws governing fault slip were well established. Modeling approaches adapted to nonlinear, chaotic systems may be best suited to tackle this challenge.

CRediT authorship contribution statement

Judith Gauriau: Conceptualization, Investigation, Data Analysis, Figure drafting, Writing – Original draft preparation. **Sylvain Barbot:** Conceptualization, Methodology, Writing – Reviewing and Editing. **James Dolan:** Conceptualization, Writing – Reviewing and Editing.

Declaration of competing interest

The authors declare that they have no known competing financial interests or personal relationships that could have appeared to influence the work reported in this paper.

Data availability

Data will be made available on request.

Acknowledgements

We thank two anonymous reviewers for useful improvements to this paper, as well as Sharadha Sathiakumar and Binhao Wang for their help with graphics. Sylvain Barbot acknowledges funding from the National Science Foundation, under award number EAR-1848192. The authors declare they have no competing interests.

Appendix A. Supplementary material

Supplementary material related to this article can be found online at https://doi.org/10.1016/j.epsl.2023.118274.

References

Akçiz, S.O., Ludwig, L.G., Arrowsmith, J.R., Zielke, O., 2010. Century-long average time intervals between earthquake ruptures of the San Andreas fault in the Carrizo Plain, California. Geology 38, 787–790. https://doi.org/10.1130/G30995.1.

Barbot, S., 2022. A rate-, state-, and temperature-dependent friction law with competing healing mechanisms. J. Geophys. Res., Solid Earth 127, e2022JB025106. https://doi.org/10.1029/2022JB025106.

Barbot, S., 2021. A spectral boundary-integral method for quasi-dynamic ruptures of multiple parallel faults. Bull. Seismol. Soc. Am. 111, 1614–1630. https://doi.org/10.1785/0120210004.

Barbot, S., 2020. Frictional and structural controls of seismic super-cycles at the Japan trench. Earth Planets Space 72, 63. https://doi.org/10.1186/s40623-020-01185-3.

Barbot, S., 2019a. Modulation of fault strength during the seismic cycle by grain-size evolution around contact junctions. Tectonophysics 765, 129–145.

Barbot, S., 2019b. Slow-slip, slow earthquakes, period-two cycles, full and partial ruptures, and deterministic chaos in a single asperity fault. Tectonophysics 768, 228171. https://doi.org/10.1016/j.tecto.2019.228171.

Barth, N.C., Kulhanek, D.K., Beu, A.G., Murray-Wallace, C.V., Hayward, B.W., Mildenhall, D.C., Lee, D.E., 2014. New c. 270 kyr strike-slip and uplift rates for the southern Alpine Fault and implications for the New Zealand plate boundary. J. Struct. Geol. 64, 39–52.

Becker, T., 2000. Deterministic chaos in two state-variable friction sliders and the effects of elastic interactions. In: Geocomplexity and the Physics of Earthquakes, vol. 120. AGU.

Beeler, N.M., Tullis, T.E., Goldsby, D.L., 2008. Constitutive relationships and physical basis of fault strength due to flash heating. J. Geophys. Res., Solid Earth 113. https://doi.org/10.1029/2007JB004988.

Berryman, K.R., Beanland, S., Cooper, A.F., Cutten, H.N., Norris, R.J., Wood, P.R., 1992. The Alpine Fault, New Zealand: variation in Quaternary structural style and geomorphic expression. Ann. Tecton. 6, 126–163.

Berryman, K.R., Cochran, U.A., Clark, K.J., Biasi, G.P., Langridge, R.M., Villamor, P., 2012. Major earthquakes occur regularly on an isolated plate boundary fault. Science 336, 1690–1693. https://doi.org/10.1126/science.1218959.

Blanpied, M.L., Lockner, D.A., Byerlee, J.D., 1995. Frictional slip of granite at hydrothermal conditions. J. Geophys. Res., Solid Earth 100, 13045–13064. https://doi.org/10.1029/95JB00862.

Boulton, C., Carpenter, B.M., Toy, V., Marone, C., 2012. Physical properties of surface outcrop cataclastic fault rocks, Alpine Fault, New Zealand. Geochem. Geophys. Geosyst. 13. https://doi.org/10.1029/2011GC003872.

Boulton, C., Moore, D.E., Lockner, D.A., Toy, V.G., Townend, J., Sutherland, R., 2014. Frictional properties of exhumed fault gouges in DFDP-1 cores, Alpine Fault, New Zealand. Geophys. Res. Lett. 41, 356–362. https://doi.org/10.1002/2013GL058236.

Boulton, C., Yao, L., Faulkner, D.R., Townend, J., Toy, V.G., Sutherland, R., Ma, S., Shimamoto, T., 2017. High-velocity frictional properties of Alpine Fault rocks: mechanical data, microstructural analysis, and implications for rupture propagation. J. Struct. Geol. 97, 71–92. https://doi.org/10.1016/j.jsg.2017.02.003.

Byerlee, J., 1978. Friction of rocks. In: Byerlee, D., Wyss, M. (Eds.), Rock Friction and Earthquake Prediction. In: Contributions to Current Research in Geophysics (CCRG). Birkhäuser, Basel, pp. 615–626.

Cattania, C., 2019. Complex earthquake sequences on simple faults. Geophys. Res. Lett. 46, 10384–10393. https://doi.org/10.1029/2019GL083628.

Cochran, U.A., Clark, K.J., Howarth, J.D., Biasi, G.P., Langridge, R.M., Villamor, P., Berryman, K.R., Vandergoes, M.J., 2017. A plate boundary earthquake record from a wetland adjacent to the Alpine fault in New Zealand refines hazard estimates. Earth Planet. Sci. Lett. 464, 175–188. https://doi.org/10.1016/j.epsl.2017.02.026.

Collettini, C., Niemeijer, A., Viti, C., Marone, C., 2009. Fault zone fabric and fault weakness. Nature 462, 907–910. https://doi.org/10.1038/nature08585.

Copley, A., 2018. The strength of earthquake-generating faults. J. Geol. Soc. 175, 1–12. https://doi.org/10.1144/jgs2017-037.

De Pascale, G.P., Langridge, R.M., 2012. New on-fault evidence for a great earthquake in A.D. 1717, central Alpine fault, New Zealand. Geology 40, 791–794. https://doi.org/10.1130/G33363.1.

De Santis, A., Cianchini, G., Qamili, E., Frepoli, A., 2010. The 2009 L'Aquila (central Italy) seismic sequence as a chaotic process. Tectonophysics 496, 44–52. https://doi.org/10.1016/j.tecto.2010.10.005.

Dieterich, J.H., 1979. Modeling of rock friction: 1. Experimental results and constitutive equations. J. Geophys. Res., Solid Earth 84, 2161–2168. https://doi.org/10.1029/JB084iB05p02161.

Erickson, B., Birnir, B., Lavallée, D., 2008. A model for aperiodicity in earthquakes. Nonlinear Process. Geophys. 15, 1–12. https://doi.org/10.5194/npg-15-1-2008.

Ferry, M., Meghraoui, M., Karaki, N.A., Al-Taj, M., Khalil, L., 2011. Episodic behavior of the Jordan valley section of the Dead Sea fault inferred from a 14-ka-long integrated catalog of large earthquakes. Bull. Seismol. Soc. Am. 101, 39–67.

Gauriau, J., Dolan, J.F., 2021. Relative structural complexity of plate-boundary fault systems controls incremental slip-rate behavior of major strike-slip faults. Geochem. Geophys. Geosyst. 22. https://doi.org/10.1029/2021GC009938.

Gualandi, A., Faranda, D., Marone, C., Cocco, M., Mengaldo, G., 2023. Deterministic and stochastic chaos characterize laboratory earthquakes. Earth Planet. Sci. Lett. 604, 117995. https://doi.org/10.1016/j.epsl.2023.117995.

Howarth, J.D., Barth, N.C., Fitzsimons, S.J., Richards-Dinger, K., Clark, K.J., Biasi, G.P., Cochran, U.A., Langridge, R.M., Berryman, K.R., Sutherland, R., 2021. Spatiotemporal clustering of great earthquakes on a transform fault controlled by geometry. Nat. Geosci. 14, 314–320. https://doi.org/10.1038/s41561-021-00721-4.

Howarth, J.D., Cochran, U.A., Langridge, R.M., Clark, K., Fitzsimons, S.J., Berryman, K., Villamor, P., Strong, D.T., 2018. Past large earthquakes on the Alpine Fault: paleoseismological progress and future directions. N.Z. J. Geol. Geophys. 61, 309–328. https://doi.org/10.1080/00288306.2018.1464658.

Howarth, J.D., Fitzsimons, S.J., Norris, R.J., Langridge, R., Vandergoes, M.J., 2016. A 2000 yr rupture history for the Alpine fault derived from Lake Ellery, South Island, New Zealand. Geol. Soc. Am. Bull. 128, 627–643. https://doi.org/10.1130/B31300.1.

Huang, J., Turcotte, D.L., 1990. Are earthquakes an example of deterministic chaos? Geophys. Res. Lett. 17, 223–226. https://doi.org/10.1029/GL017i003p00223.

Ikari, M.J., Carpenter, B.M., Kopf, A.J., Marone, C., 2014. Frictional strength, rate-dependence, and healing in DFDP-1 borehole samples from the Alpine Fault, New Zealand. Tectonophysics 630, 1–8. https://doi.org/10.1016/j.tecto.2014.05.005.

Iliopoulos, A.C., Pavlos, G.P., 2010. Global low dimensional seismic chaos in the Hellenic region. Int. J. Bifurc. Chaos 20, 2071–2095. https://doi.org/10.1142/S0218127410026939.

Ito, K., 1980. Periodicity and chaos in great earthquake occurrrence. J. Geophys. Res., Solid Earth 85, 1399–1408. https://doi.org/10.1029/JB085iB03p01399.

Kagan, Y.Y., Jackson, D.D., 1991. Long-term earthquake clustering. Geophys. J. Int. 104, 117–133. https://doi.org/10.1111/j.1365-246X.1991.tb02498.x.

Kanamori, H., Rivera, L., 2006. Energy Partitioning During an Earthquake. American Geophysical Union, Washington, DC, pp. 3–13. https://resolver.caltech.edu/CaltechAUTHORS:20110629-112907012. (Accessed December 2022).

Kato, N., 2014. Deterministic chaos in a simulated sequence of slip events on a single isolated asperity. Geophys. J. Int. 198, 727–736. https://doi.org/10.1093/gji/ggu157.

Kondo, H., Özaksoy, V., Yıldirim, C., 2010. Slip history of the 1944 Bolu-Gerede earthquake rupture along the North Anatolian fault system: implications for recurrence behavior of multisegment earthquakes. J. Geophys. Res. 115.

Langridge, R., et al., 2016. The New Zealand active faults database. N.Z. J. Geol. Geophys. 59, 86–96. https://doi.org/10.1080/00288306.2015.1112818.

Li, T.-Y., Yorke, J.A., 2004. Period three implies chaos. In: Hunt, R., Li, T.-Y., Kennedy, J.A., Nusse, H.E. (Eds.), The Theory of Chaotic Attractors. Springer, New York, NY, pp. 77–84.

Lorenz, E.N., 1963. Deterministic nonperiodic flow. J. Atmos. Sci. 20, 130–141. https://doi.org/10.1175/1520-0469(1963)020<0130:DNF>2.0.CO;2.

Marco, S., Stein, M., Agnon, A., Ron, H., 1996. Long-term earthquake clustering: a 50,000-year paleoseismic record in the Dead Sea Graben. J. Geophys. Res., Solid Earth 101, 6179–6191. https://doi.org/10.1029/95JB01587.

Nie, S., Barbot, S., 2022. Rupture styles linked to recurrence patterns in seismic cycles with a compliant fault zone. Earth Planet. Sci. Lett. 591, 117593. https://doi.org/10.1016/j.epsl.2022.117593.

Nie, S., Barbot, S., 2021. Seismogenic and tremorgenic slow slip near the stability transition of frictional sliding. Earth Planet. Sci. Lett. 569, 117037. https://doi.org/10.1016/j.epsl.2021.117037.

Noda, H., Lapusta, N., 2013. Stable creeping fault segments can become destructive as a result of dynamic weakening. Nature 493, 518–521. https://doi.org/10.1038/nature11703.

Rice, J.R., Ruina, A.L., 1983. Stability of steady frictional slipping. J. Appl. Mech. 50, 343–349. https://doi.org/10.1115/1.3167042.

Rockwell, T.K., Dawson, T.E., Young Ben-Horin, J., Seitz, G., 2015. A 21-event, 4,000-year history of surface ruptures in the Anza seismic gap, San Jacinto fault, and implications for long-term earthquake production on a major plate boundary fault. Pure Appl. Geophys. 172, 1143–1165. https://doi.org/10.1007/s00024-014-0955-z.

Rubin, A.M., Ampuero, J. 3-D Earthquake Nucleation on Rate-and-State Faults, p. T13E-07.

Ruina, A., 1983. Slip instability and state variable friction laws. J. Geophys. Res., Solid Earth 88, 10359–10370. https://doi.org/10.1029/JB088iB12p10359.

Sathiakumar, S., Barbot, S., 2021. The stop-start control of seismicity by fault bends along the Main Himalayan Thrust. Commun. Earth Environ. 2, 1–11. https://doi.org/10.1038/s43247-021-00153-3.

Scharer, K.M., Biasi, G.P., Weldon II, R.J., 2011. A reevaluation of the Pallett Creek earthquake chronology based on new AMS radiocarbon dates, San Andreas fault, California. J. Geophys. Res., Solid Earth 116. https://doi.org/10.1029/2010JB008099.

Shelly, D.R., 2010. Periodic, chaotic, and doubled earthquake recurrence intervals on the deep San Andreas fault. Science 328, 1385–1388. https://doi.org/10.1126/science.1189741.

Shimazaki, K., Nakata, T., 1980. Time-predictable recurrence model for large earthquakes. Geophys. Res. Lett. 7, 279–282. https://doi.org/10.1029/GL007i004p00279.

Stirling, M., et al., 2012. National seismic hazard model for New Zealand: 2010 UpdateNational seismic hazard model for New Zealand: 2010 update. Bull. Seismol. Soc. Am. 102, 1514–1542. https://doi.org/10.1785/0120110170.

Sulem, J., Famin, V., 2009. Thermal decomposition of carbonates in fault zones: slip-weakening and temperature-limiting effects. J. Geophys. Res., Solid Earth 114. https://doi.org/10.1029/2008JB006004.

Sutherland, R., et al., 2007. Do great earthquakes occur on the Alpine Fault in central South Island, New Zealand?. In: Okaya, D., Stern, T., Davey, F. (Eds.), Geophysical Monograph Series, vol. 175. American Geophysical Union, Washington, D.C., pp. 235–251.

Sutherland, R., Berryman, K.R., Norris, R., 2006. Quaternary slip rate and geomorphology of the Alpine fault: implications for kinematics and seismic hazard in southwest New Zealand. Geol. Soc. Am. Bull. 118, 464–474.

Tse, S.T., Rice, J.R., 1986. Crustal earthquake instability in relation to the depth variation of frictional slip properties. J. Geophys. Res., Solid Earth 91, 9452–9472. https://doi.org/10.1029/JB091iB09p09452.

Valdez II, R., Kitajima, H., Saffer, D., 2019. Effects of temperature on the frictional behavior of material from the Alpine Fault Zone, New Zealand. Tectonophysics 762, 17–27. https://doi.org/10.1016/j.tecto.2019.04.022.

Wang, L., Barbot, S., 2020. Excitation of San Andreas tremors by thermal instabilities below the seismogenic zone. Sci. Adv. 6, eabb2057. https://doi.org/10.1126/sciadv.abb2057.

Wang, B., Barbot, S., 2023. Pulse-like ruptures, seismic swarms, and tremorgenic slow-slip events with thermally activated friction. Earth Planet. Sci. Lett. 603, 117983. https://doi.org/10.1016/j.epsl.2022.117983.

Wechsler, N., Rockwell, T.K., Klinger, Y., Štěpančíková, P., Kanari, M., Marco, S., Agnon, A., 2014. A paleoseismic record of earthquakes for the dead sea transform fault between the first and seventh centuries C.E.: nonperiodic behavior of a plate boundary fault. Bull. Seismol. Soc. Am. 104, 1329–1347. https://doi.org/10.1785/0120130304.

Weldon, R., Scharer, K., Fumal, T., Biasi, G., 2004. Wrightwood and the earthquake cycle: what a long recurrence record tells us about how faults work. GSA Today 14, 4–10.

Yetton, M.D., Nobes, D.C., 1998. Recent vertical offset and near-surface structure of the Alpine Fault in Westland, New Zealand, from ground penetrating radar profiling. N.Z. J. Geol. Geophys. 41, 485–492. https://doi.org/10.1080/00288306.1998.9514825.